

Drop Size Distributions and the Lack of Small Drops in RICO Rain Shafts

BRAD BAKER, QIXU MO, R. PAUL LAWSON, AND DARREN O'CONNOR

SPEC, Inc., Boulder, Colorado

ALEXEI KOROLEV

Environment Canada, Downsview, Ontario, Canada

(Manuscript received 3 December 2007, in final form 9 June 2008)

ABSTRACT

Data from the new two-dimensional stereo (2D-S) probe are used to evaluate drop size distributions in rain shafts observed during the Rain in Shallow Cumulus over the Ocean (RICO) experiment. The 2D-S takes images of both precipitation drops and cloud droplets with 10- μm resolution. These are the first reported measurements of rain to include sizes smaller than 100 μm . The primary result is that there are almost no hydrometeors smaller than about 100 μm in these rain shafts. The measured low concentration of small hydrometeors implies that their rate of production is slow relative to their removal rate. Algorithms for removing the spurious effects of splashing precipitation and noisy photodiodes on 2D probes are also described.

1. Introduction

Data from the new SPEC, Inc., two-dimensional stereo (2D-S) probe (Lawson et al. 2006) are used to evaluate drop size distributions (DSDs) in rain shafts observed during the Rain In Shallow Cumulus over the Ocean (RICO; Rauber et al. 2007) experiment. These are the first reported measurements of rain DSDs to include sizes smaller than 100 μm . The primary result is that there are almost no hydrometeors smaller than about 100 μm in RICO rain shafts. This manuscript also addresses the task of removing the effects of precipitation splashing off 2D probe tips and causing spurious images commonly referred to as "artifacts." The spurious effects of precipitation on the forward scattering spectrometer probe (FSSP), King hot-wire, and particle volume monitor probes will be documented in a follow-on paper, using the same RICO data.

For several decades, the cloud physics community has expressed concern that both ice and water particles may be shattering on the inlets of airborne particle probes, creating artifacts that introduce errors in measurements of particle size distributions. Airborne measurements of

drop size distributions in rain shafts have been inherently prone to errors caused by drops splashing on the probe tips of optical imaging probes (Heymsfield and Baumgardner 1985). When ice particle shattering and drop splashing occur and contribute significant errors in particle size distributions (PSDs), the results not only confound physical interpretation of cloud processes but also introduce ramifications that ripple through derived parameters. For example, an artificial increase in small particles could have a significant impact on derived radiative properties, such as extinction and effective particle radius, two parameters used in radiative transfer calculations and global climate model predictions.

Because all of the particle size spectrometers currently in use are subject to spurious measurements from splashing precipitation, only those probes that allow discrimination between valid and spurious counts can be reliably used in precipitation. Shortly after the introduction of the Particle Measuring Systems, Inc., (PMS) particle imaging probes (Knollenberg 1970), Cooper (1978) suggested using interarrival time (i.e., the time of arrival between particles) to help to eliminate spurious particle images caused by breakup of particles on impact with the PMS probe tips. The concept is that closely grouped particles are generated by an ice particle that has shattered or from a drop that has splashed upon impact with a probe inlet or probe tip.

Corresponding author address: Brad Baker, SPEC, Inc., 3022 Sterling Circle, Suite 200, Boulder, CO 80301.
E-mail: brad@specinc.com

Analyses using interarrival time to estimate the effects of particles shattering on PMS 2D probe tips have been conducted (Korolev and Isaac 2005; Field et al. 2006). Korolev and Isaac limited their analysis to probes that measure only precipitation size particles and estimated that the increase in number concentration from ice particle shattering does not exceed about 10%. Field et al. (2006) estimated that the number concentration of the PMS cloud particle-imaging probe (2D-C) is increased by up to a factor of 4. However, although the PMS imaging probes are capable of measuring the larger particles, because of time-response limitations, Lawson et al. (2006) showed that the 2D-C, installed on the National Center for Atmospheric Research (NCAR) C-130 research aircraft used in the RICO project, was not able to image particles smaller than about $100 \mu\text{m}$ at 100 m s^{-1} . Lawson et al. (2006) show data suggesting that particles that appear to be smaller than about $100 \mu\text{m}$ are likely a result of larger particles that are poorly imaged because of slow time response and diffraction effects. It is important to note that the percentage increase in measured number concentration caused by shattering may vary enormously from one cloud situation to another because it depends on the natural concentration, which is typically dominated by small particles, as well as on the concentration of spurious (shattered) particles, which depends primarily on the concentration of large particles.

Ground-based measurements of precipitation (e.g., Low and List 1982) have generally been accomplished using the Joss–Waldvogel drop distrometer (Joss and Waldvogel 1967), which has a drop threshold size of about $200 \mu\text{m}$ (Sheppard and Joe 1994; Tokay et al. 2001). Sheppard and Joe (1994) show surface measurements in precipitation using a $150\text{-}\mu\text{m}$ resolution gray probe (Joe and List 1987). Tokay et al. (2001) show surface precipitation measurements from a two-dimensional video distrometer (2DVD), described by Schöhuber et al. (1997). The 2DVD measures drops with a minimum diameter of about $200 \mu\text{m}$. Thus, reliable measurements of small drops (i.e., drops with diameters of less than about $100 \mu\text{m}$) in rain shafts are absent from the literature. In this study, 2D-S data are used to determine the concentration of droplets, down to about $10 \mu\text{m}$ diameter, that occur naturally in RICO rain shafts.

One of the goals of RICO, which took place over December 2004–February 2005 near Antigua, was to study the development of precipitation in shallow, warm, tropical cumulus clouds. The 2D-S probe flew on the NCAR C-130 research aircraft, along with NCAR's 2D-C. The C-130 made hundreds of penetrations of cumulus clouds and rain shafts beneath clouds, collecting measurements that are used here to evaluate the

drop size distributions in rain shafts. Section 2 presents some salient features of the 2D-S probe, section 3 shows examples of precipitation images and spurious images caused by splashing in a rain shaft and presents 2D-S measurements of rain-shaft PSDs that indicate that a dearth of small droplets exist in RICO rain shafts. Section 4 discusses explanations for the observations and modeling work thereon. Section 5 summarizes the conclusions of this research.

2. Salient features of the 2D-S probe

The 2D-S probe utilizes a new 128-element linear photodiode array that was custom fabricated to improve time response. The 2D-S optics are configured to produce $10\text{-}\mu\text{m}$ pixels in the 2D-S sample volume. The arrival time of each particle imaged by the 2D-S is recorded at a precision commensurate with $10\text{-}\mu\text{m}$ spatial resolution. Lawson et al. (2006) show results of laboratory tests using a high-speed spinning fiber demonstrating that the improved time response allows the 2D-S to respond quickly enough to image individual $10\text{-}\mu\text{m}$ droplets at aircraft speeds. To demonstrate this ability more directly, a comparison of 2D-S and FSSP PSDs is shown in Fig. 1. This comparison is made in clear air at 300-ft ($\sim 91 \text{ m}$) altitude over the ocean near Antigua for a 30-min period during which there were no clouds overhead and no falling precipitation. In this situation, the probes are detecting only deliquesced aerosol. The maximum diameter according to the FSSP, which sizes droplets into 15 size bins between 3 and $45 \mu\text{m}$, is about $18 \mu\text{m}$. This eliminates the possibility that the 2D-S is incorrectly sizing larger particles as 10 and $20 \mu\text{m}$. The 2D-S appears to oversize a few, as should be expected from diffraction effects of out-of-focus images (Korolev et al. 1998).¹ The first bin of the 2D-S (single pixel images) is nominally assigned bin edges from 5 to $15 \mu\text{m}$. Given that true $5\text{-}\mu\text{m}$ -diameter droplets have a significantly lower detection probability than true $15\text{-}\mu\text{m}$ -diameter droplets, the 2D-S measures a reasonable number in comparison with the FSSP. Sampling statistics

¹ Two methods of dealing with out-of-focus miss-sizing effects have been applied to the RICO 2D-S data. One method is to use only in-focus (\sim solid-appearing) images, the other uses the Korolev et al. (1998) corrections. Results are similar enough between the methods that the conclusions herein would not be altered according to the method used. The in-focus only method was used for the processing presented in this manuscript. The diameters of drops larger than about 300 microns are estimated using the size measured along the direction of travel to improve sampling statistics. Smaller particle diameters are estimated from the size along the array.

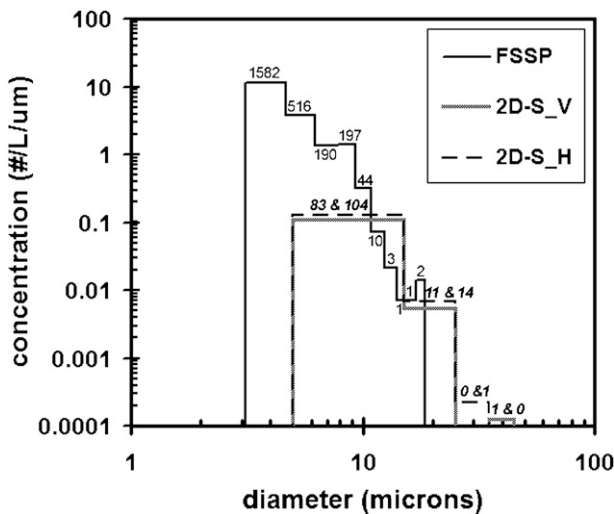


FIG. 1. Comparison of the 2D-S (H and V channels) with the FSSP during clear-air sampling of deliquesced aerosol at 300 ft (91 m) on 19 Jan 2005 from 1828 to 1858. The number of actual counts in each bin is written above or below each bar, with 2D-S counts in boldface italic.

are poor for both the FSSP and the 2D-S in this situation (the actual counts are displayed on the figure); therefore, the agreement could be coincidental. However, the 2D-S horizontal (H) and vertical (V) channels represent independent measurements, thus three independent measurements agree. This provides us enough confidence to interpret counts in the first two bins of the 2D-S as deliquesced aerosol in the rain shafts (discussed later).

Thus, the 2D-S is capable of imaging and recording the arrival times of both cloud droplets and precipitation and therefore provides a more complete dataset for quantifying the drop size distributions in rain shafts than was previously available. Because the 2D-S probe records images and arrival times of thousands of drops before going into overload, it is reasonably straightforward to use interarrival times to filter out images that result from splashing.

3. Measurements of drop size distributions in RICO rain shafts

Splashing events on the 2D-S are a regular occurrence in the presence of raindrops and are easily identified by visual inspection of the 2D-S images. As shown in Fig. 2, groups of images close together are identified as splashing events. Visual inspection also suggests that there are very few natural cloud-droplet-sized drops. That is, all of the small drops are associated with the clearly identifiable splashing events. However, visual inspection restricts the analysis to a very small amount of

data. We analyze large data segments automatically using the distance between the images to distinguish natural versus splashing drops. This approach was originally proposed by Cooper (1978) and has been used to estimate the number of small particles produced by shattered ice particles (Korolev and Isaac 2005; Field et al. 2006) but to date has not been used to quantify the effects of drop splashing on 2D probes.

The distances between spurious drops caused by splashing are, on average, very much smaller than the distances between natural drops (Fig. 2) and thus may be used to distinguish between artifacts and real 2D-S images. However, the individual distances between drops are approximately exponentially distributed (the so-called waiting-time distribution) for both types of events. Therefore, there is no unique cutoff distance that perfectly segregates the data into spurious and natural drops. We studied the effect of varying cutoff values and found that by 1 or 2 cm effectively all splashing effects are removed, which is consistent with the values found and used by Cooper (1978) and Field et al. (2006). However, in dense cumulus cloud such a cutoff would remove a high percentage of valid images as well. Therefore, we use a variable cutoff value of 2 cm or less, depending on the local concentration and depending on whether precipitation exists. An adjustment for the valid images inadvertently removed by the cutoff criteria is applied assuming Poisson statistics. Additional rejection criteria remove spurious events caused by noisy photodiodes. A description of the artifact removal algorithms is provided in appendix A.

Figure 3 shows an example of a PSD that is an average over 2 min of continuous rain. The main graph shown in Fig. 3 demonstrates the magnitude of the effects of splashing drops and noisy photodiodes by presenting three PSDs with increasing degrees of artifact removal. The light-gray trace shows the PSD with no artifact removal. The thin black trace shows the PSD after removal of signals from noisy photodiodes. The dark-gray trace shows the PSD after removal of signals from noisy photodiodes and images resulting from splashing drops (i.e., full artifact removal). Each of these PSDs was calculated as the average of the individual independent PSDs estimated from the two channels of the 2D-S. The inset graph of Fig. 3 shows the independent PSDs from each channel (H and V) of the 2D-S separately, with full artifact removal. Also shown in the inset of Fig. 3 are the PSDs from the 2D-C and 2D-P that were operated on the NCAR C-130. These data are processed to remove splashing events using techniques described in Korolev and Isaac (2005). The details of those techniques as applied to these data are presented in appendix B. The points we wish to express with this figure are 1) that

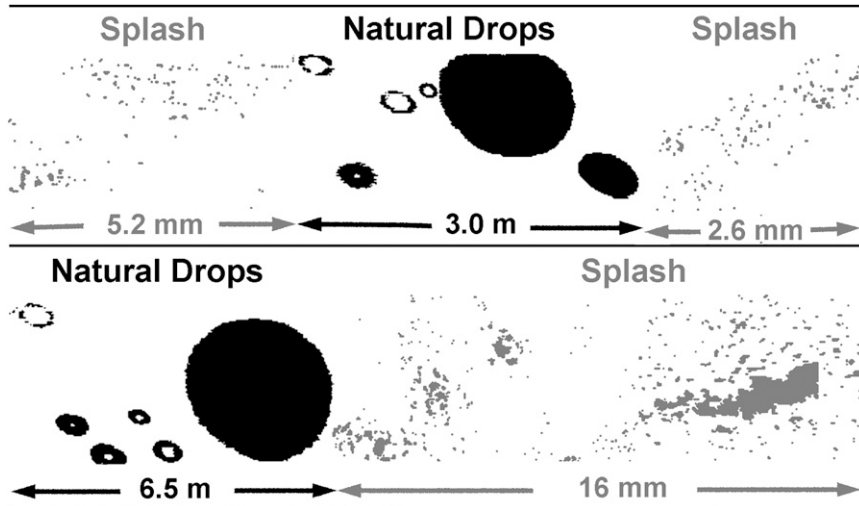


FIG. 2. Typical images, from the 2D-S probe, of natural precipitation drops (black) and spurious images from splashing of drops off the probe tips (gray). The white space representing distances between images is not shown, but the actual distances over which the images were obtained are shown. Note that spurious image distances are labeled in millimeters, and natural drops' image distances are labeled in meters. Also, note that the 2D-S images of real drops tend to be slightly ellipsoidal. This is due to an inadvertent 11° tilt of the arrays during RICO that has subsequently been corrected. The ellipsoidal shapes in the RICO dataset are accounted for in software.

there are very few particles with size between about 30 and $100 \mu\text{m}$, 2) that, while the noise rejection is noticeable, the major contributor of spurious particles is splashing, 3) that the two (H and V) channels of the 2D-S measure very nearly the same PSD, and 4) that there is a less-tight agreement between the 2D-S PSDs and the PMS probes' (2D-C and 2D-P) PSDs. Some comparisons with other 2D imaging probes can be found in Lawson et al. (2006).

The principle of operation of the 2D-S is the same as the older 2D-C and 2D-P probes. The main difference in the probes is the improved time response and spatial resolution of the 2D-S. Thus, we expect the 2D-S to provide the most reliable data with the possible exception of the largest sizes. For the largest-sized particles, we expect the 2D-P could provide more reliable data because of its larger sample volume and therefore better sampling statistics. This is especially of concern because image reconstruction techniques have not yet been implemented for the 2D-S. The 2D-S does fall somewhat below the 2D-P at the largest sizes, which is consistent with the hypothesis that the 2D-S is undersizing the largest drops as a result of not using image reconstruction techniques. However, the lack of agreement between the 2D-S PSD and the 2D-C and 2D-P PSDs is as large or larger at other sizes, and thus no firm conclusions about the causes of the disagreement can be made at any of the sizes.

To demonstrate the generality of the result that there are very few droplets smaller than about $100 \mu\text{m}$ in the RICO rain shafts, we present, in Fig. 4, information from 237 rain-shaft segments. The 237 rain shafts were sampled at 600 ft ($\sim 183 \text{ m}$) altitude on 19 January 2005. Rain shafts were determined by the following criteria. The segment must be at least 3 s long ($\sim 300 \text{ m}$) during which the FSSP concentration remains within 0.8 and 1.2 times the mean FSSP concentration for the same period and the 2D-C and 2D-P precipitation water content remains within 0.5 and 1.5 of its mean for the same period. This allows the automation of the processing, removes human biases, and insures some degree of uniformity over the averaging regions. For the rain-shaft determination, the data were taken from the NCAR-released netcdf-format data files. Incomplete artifact rejection was applied to these 2D data, and thus absolute values can be erroneously high. However, for the purpose here of determining the rain-shaft segments the data are adequate.

The individual PSDs are too numerous to distinguish if plotted together. Therefore, we plot density contours of values of those 237 PSDs. It can be seen that there is a wide spread of values and thus a variety of shapes and magnitudes within the 237 PSDs. Most notable however, is that only a few register counts in the bins between about 30 and $100 \mu\text{m}$. A greater number of the PSDs register a few counts in the first and second bins

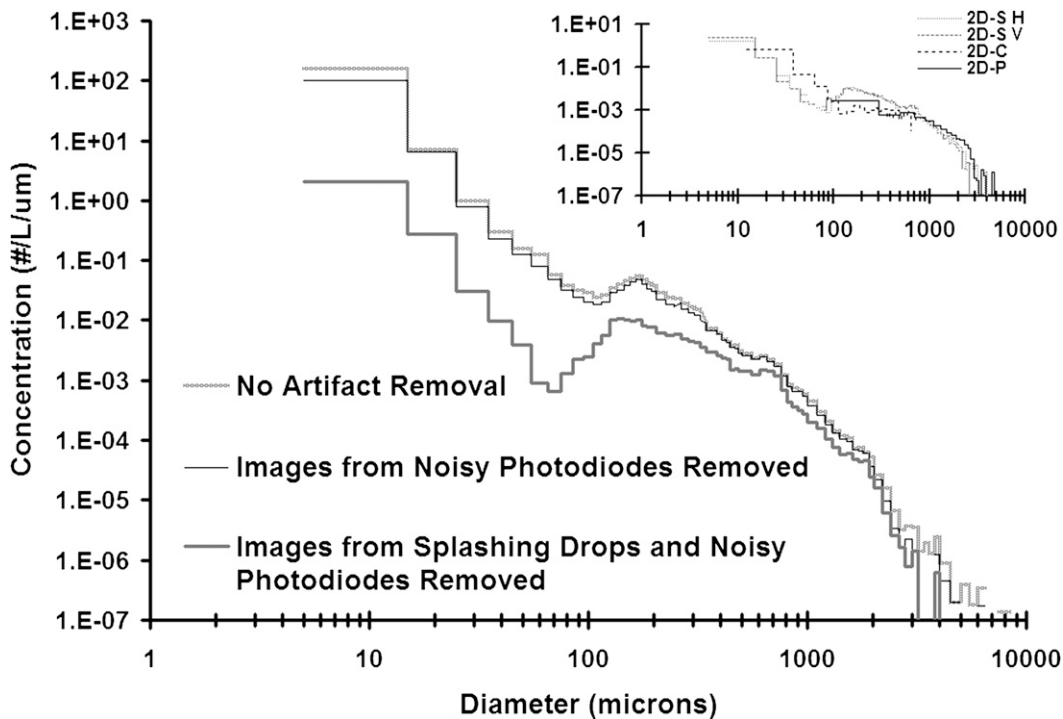


FIG. 3. Comparison of PSDs showing effects of artifact removal on measurements collected in rain by the NCAR C-130 from 1442:04 to 1444:04 1 Jan 2005. The 2D-S PSDs in the main graph show no artifact removal (light gray), noisy photodiodes removed (thin black), and both noisy photodiodes and splashing effects removed, i.e., full artifact removal (dark gray). Inset shows comparison of 2D-S V- and H-channel PSDs, with artifact removal, and 2D-C and 2D-P PSDs with artifact removal.

(10 and 20 μm). These are most likely deliquesced aerosols. The few counts leading to nonzero values in the dip region (30 and 100 μm) may be natural particles, such as rare deliquesced ultragiant nuclei or remnants of recent natural drop breakup. However, they may also be rare artifacts not removed by the artifact removal algorithm (appendix A), including out-of-focus larger particles that appear as one or more smaller particles. Therefore, the uncertainty in the concentration of drops between 30 and 100 μm is as large as the estimate itself. The estimates in both Figs. 3 and 4 are of less than 1 L^{-1} but the true value may be anything less.

Rain shafts at other altitudes [300, 800, and 1000 ft (1 ft $\cong 30.5 \text{ cm}$)] were similarly analyzed with no significant differences in the results.

4. Discussion

The result of this work is that there are relatively few, if any, drops smaller than about 100 μm in the RICO rain shafts studied. Size-dependent fall velocities cause separation between cloud and precipitation. It is possible that drop breakup (Pruppacher and Klett 1997, section 10.3.5) creates small drops. Another source of

drops smaller than 100 μm is evaporation of drops larger than 100 μm . It is apparent that these generation processes are slow relative to the removal processes so that the net concentration of drops smaller than 100 μm remains low. Removal processes are complete evaporation in the generally subsaturated² rain-shaft air and collision and coalescence, which can return the small drop mass to a larger size drop. Correlations between the low concentrations of deliquesced aerosol, the low concentrations of drops between 30 and 100 μm , the relative humidity, and the vertical velocities might be expected in this situation. Vertical velocities range primarily between $\pm 1 \text{ m s}^{-1}$, however no such correlations are found in this dataset. The largest drops in the RICO rain shafts were about 3 mm, and so these findings may

² All of the rain shaft segments selected by the algorithm described in section 3 were subsaturated. Supersaturation can be reached below cloud base in localized regions where conditions, in particular an updraft, allow it. In such a region many small droplets may form. We observed this phenomenon in one location below cloud base that was not selected by the rain shaft segment algorithm. It thus appears to be rare and not generally relevant to the description of the RICO rain shafts.

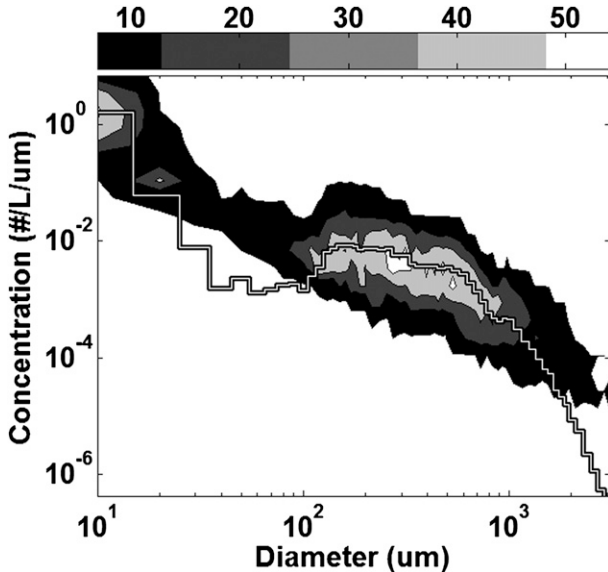


FIG. 4. The mean of 237 rain PSDs is shown on top of density contours of the 237 individual rain PSDs observed at 600-ft (~ 183 m) altitude over the ocean on 19 Jan 2005. The contours show the number of PSDs passing through the region. Very few individual PSDs have any counts at all between 30 and 100 μm . These do not appear on the contour plot because zero values are not included on log-log plots.

not extend to all rain shafts. Rain shafts with larger drops may contain greater numbers of drops $< 100 \mu\text{m}$, possibly because of more vigorous drop breakup.

Studies modeling these physical processes (Nicholls 1987, List and McFarquhar 1990) predict a lack of smaller drops below cloud, similar to the observations presented herein. Nicholls (1987) also shows observational measurements of smaller drops in excess of those predicted by the model and in excess of those found in this study. Nicholls (1987) suggests that simplifications in the below-cloud model were responsible for the discrepancies. In light of what we now know, that all probes can be significantly affected by precipitation unless some means of removing those effects are employed, an alternative explanation for the discrepancies exists. The subcloud measurements of smaller drops were likely spurious effects of the precipitation on the probes used to measure the smaller drops [an axially scattering spectrometer probe, a Johnson–Williams hot-wire probe, and a 2D imaging probe; described in Nicholls (1984)].

5. Conclusions

The main conclusion from this study is the lack of 30–100- μm -diameter cloud drops in the RICO rain shafts. There is a low concentration of deliquesced aerosols

showing up in the 10- and 20- μm size bins of the 2D-S. The concentration measurements between 30 and 100 μm are even lower than the deliquesced aerosols concentrations. The counts in these bins might be rare real particles but could also be rare spurious artifacts not completely removed by the artifact removal algorithms. The measured low concentration of hydrometeors smaller than 100 μm implies that their rate of production, through evaporation and through natural drop breakup, is slow relative to their removal rate, through evaporation and through collision and coalescence. This paper also presents data from the new 2D-S probe, including the removal of spurious effects of noisy photodiodes and splashing precipitation.

Acknowledgments. The authors thank Robert Rauber, Bjorn Stevens, Charles Knight, and Harry Oaks for the outstanding job they did in planning and executing the field phase of RICO. This work was supported under NSF Grant ATM –0342486. The SPEC 2D-S probe was developed under SBIR N00014-02-C-0317 sponsored by the Office of Naval Research Naval Postgraduate School Center for Interdisciplinary Remotely-Piloted Aircraft Studies (CIRPAS). We extend our appreciation for the support of Bob Bluth and Haffliði Jonsson.

APPENDIX A

Removing Spurious 2D-S Events

2D-S raw data include spurious effects. These are primarily from noisy photodiodes and from splashing or shattering of precipitation. Algorithms used to remove the majority of these spurious effects while retaining a majority of the valid images are briefly described herein. For a complete description, visit <http://specinc.com/> and/or contact SPEC personnel.

There are five quasi-independent steps to the algorithm: 1) test for noise through line and dot patterns, 2) test for noise through statistics of particle center locations, 3) test for roundness, 4) test for splashing events based on black and white area considerations, and 5) test for splashing events based on interevent-distances if the probe is in precipitation. For step 1, Fig. A1 shows some examples of noise-generated images appearing in line-plus-dot patterns. Such patterns are identified and eliminated using criteria based on various length and area parameters estimated from the images. In step 2, noisy photodiode effects are also removed based on the statistics of image center locations. When a photodiode is noisy, there are more images centered on this diode than on normal functioning photodiodes. Therefore image

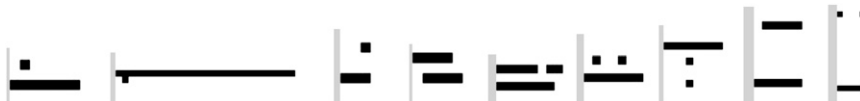


FIG. A1. Examples of line-plus-dot patterns caused by noisy photodiodes.

center location statistics are accumulated during post-processing and are used to identify noisy photodiodes. Small images located on noisy photodiodes are eliminated. Figure A2 shows an example of the distribution of image centers across the array, images kept, and images removed by this and the other artifact removal steps.

In step 3, an image is determined to be round if its aspect ratio, determined as the ratio of the size along the array to the size perpendicular to the array, is between 0.5 and 2.0. Only images determined to be round are accepted as valid images. In step 4, as can be seen in Fig. 2, images of large drops consist primarily of black pixels, whereas images of splashing events can consist of nu-

merous white pixels as well as black pixels. These facts are used to eliminate splashing images by consideration of the number of white and black pixels contained in an image. Step 5, the final step, is described in the second paragraph of section 3.

APPENDIX B

Removing Spurious 2D-C and 2D-P Events

The OAP-2DC/2DP data were analyzed with the help of 2D-processing software (<http://www.skytechresearch.com/feedback.htm>). The general approach for rejection

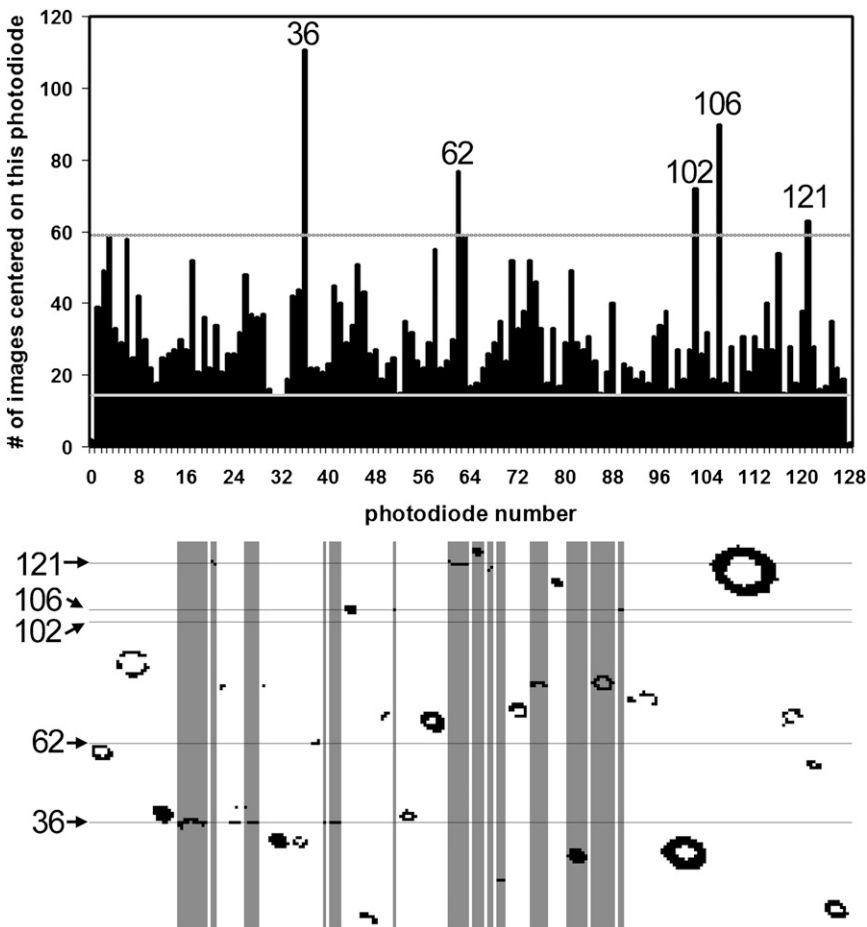


FIG. A2. (bottom) An example of noisy photodiode data intermixed with good particle data. The images highlighted in gray are rejected. Horizontal lines indicate the location of photodiodes determined to be noisy as shown in the (top) particle-center-location distribution.

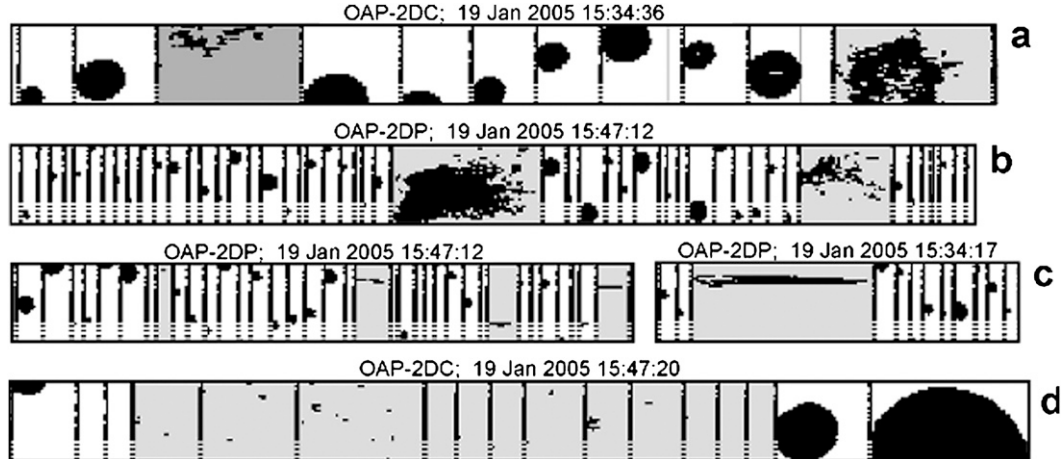


FIG. B1. Examples of OAP-2DC and OAP-2DP image frames rejected because of (a), (b) fragmented images, (c) aspect ratio, and (d) short interarrival time.

of splashing was the same as was used for the rejection of the shattered ice particles described in Korolev and Isaac (2005). The following criteria were used to segregate splashing events. A particle image frame was excluded from the analysis if 1) the image frame contained more than three isolated images^{B1} (Fig. B1a,b), 2) the aspect ratio of the image, determined as the ratio of the size perpendicular to the array to the size along the array, is greater than 2 [this criterion allows one to eliminate streakers resulting from splashing (Fig. B1c)], and 3) the distance between two successive particles is less than 1 cm (Fig. B1d), which corresponds to approximately 100 μ s of interarrival time between particles at a speed of 100 m s⁻¹.

REFERENCES

- Cooper, W. A., 1978: Cloud physics investigations by the University of Wyoming in HIPLEX 1977. Department of Atmospheric Science, University of Wyoming, Rep. AS119, 320 pp.
- Field, P. R., A. J. Heymsfield, and A. Bansemer, 2006: Shattering and particle interarrival times measured by optical array probes in ice clouds. *J. Atmos. Oceanic Technol.*, **23**, 1357–1371.
- Heymsfield, A. J., and D. Baumgardner, 1985: Summary of a workshop on processing 2-D probe data. *Bull. Amer. Meteor. Soc.*, **66**, 437–440.
- Joe, P., and R. List, 1987: Testing and performance of two-dimensional optical array spectrometers with greyscale. *J. Atmos. Oceanic Technol.*, **4**, 139–150.
- Joss, J., and A. Waldvogel, 1967: A raindrop spectrograph with automatic analysis. *Pure Appl. Geophys.*, **68**, 240–246.
- Knollenberg, R. G., 1970: The optical array: An alternative to scattering or extinction for airborne particle size determination. *J. Appl. Meteor.*, **9**, 86–103.
- Korolev, A. V., and G. A. Isaac, 2005: Shattering during sampling by OAPs and HVPS. Part I: Snow particles. *J. Atmos. Oceanic Technol.*, **22**, 528–542.
- , J. W. Strapp, and G. A. Isaac, 1998: Evaluation of the accuracy of PMS optical array probes. *J. Atmos. Oceanic Technol.*, **15**, 708–720.
- Lawson, R. P., D. O'Connor, P. Zmarzly, K. Weaver, B. A. Baker, Q. Mo, and H. Jonsson, 2006: The 2D-S (stereo) probe: Design and preliminary tests of a new airborne, high speed, high-resolution particle imaging probe. *J. Atmos. Oceanic Technol.*, **23**, 1462–1477.
- List, R., and G. M. McFarquhar, 1990: The role of coalescence and breakup in the three-peak equilibrium distribution of raindrops. *J. Atmos. Sci.*, **47**, 2274–2292.
- Low, T., and R. List, 1982: Collision coalescence and break-up of raindrops with size. *J. Atmos. Sci.*, **39**, 1591–1618.
- Nicholls, S., 1984: The dynamics of stratocumulus: aircraft observations and comparisons with a mixed layer model. *Quart. J. Roy. Meteor. Soc.*, **110**, 783–820.
- , 1987: A model of drizzle growth in warm, turbulent, stratiform clouds. *Quart. J. Roy. Meteor. Soc.*, **113**, 1141–1170.
- Pruppacher, H. R., and J. D. Klett, 1997: *Microphysics of Clouds and Precipitation*. Kluwer Academic, 954 pp.
- Rauber, R. M., and Coauthors, 2007: Rain in Shallow Cumulus over the Ocean: The RICO campaign. *Bull. Amer. Meteor. Soc.*, **88**, 1912–1928.
- Schöhuber, M., H. E. Urban, J. P. V. Poaires Baptista, W. L. Randeu, and W. Riedler, 1997: Weather radar versus 2D-video-distrometer data. *Weather Radar Technology for Water Resources Management*, B. Braga Jr. and O. Massambani, Eds., UNESCO, 159–171.
- Sheppard, B. E., and P. I. Joe, 1994: Comparison of raindrop size distribution measurements by a Joss–Waldvogel disdrometer, a PMS 2DG spectrometer, and a POSS Doppler radar. *J. Atmos. Oceanic Technol.*, **11**, 874–887.
- Tokay, A., A. Kruger, and W. F. Krajewski, 2001: Comparison of drop size distribution measurements by impact and optical disdrometers. *J. Appl. Meteor.*, **40**, 2083–2097.

^{B1} In the frame of this study the term “isolated image” is applied to a group of 8-connected pixels. Two adjoining pixels are defined as “8-connected”, if at least one of four edges or one of four corners touch, along a horizontal, vertical or diagonal direction.